

Structural aging of human neurons is the opposite of the changes in schizophrenia

Ryuta Mizutani¹, Rino Saiga¹, Yoshiro Yamamoto², Masayuki Uesugi³, Akihisa Takeuchi³, Kentaro Uesugi³, Yasuko Terada³, Yoshio Suzuki⁴, Vincent De Andrade⁵, Francesco De Carlo⁵, Susumu Takekoshi⁶, Chie Inomoto⁷, Naoya Nakamura⁷, Youta Torii⁸, Itaru Kushima^{8,9}, Shuji Iritani^{8,10}, Norio Ozaki⁸, Kenichi Oshima^{10,11}, Masanari Itokawa^{10,11}, and Makoto Arai¹¹

¹Department of Bioengineering, Tokai University, Hiratsuka, Kanagawa 259-1292, Japan

²Department of Mathematics, Tokai University, Hiratsuka, Kanagawa 259-1292, Japan

³Japan Synchrotron Radiation Research Institute (JASRI/SPring-8), Sayo, Hyogo 679-5198, Japan

⁴Photon Factory, High Energy Accelerator Research Organization KEK, Tsukuba, Ibaraki 305-0801, Japan

⁵Advanced Photon Source, Argonne National Laboratory, Lemont, IL 60439, USA

⁶Department of Cell Biology, Tokai University School of Medicine, Isehara, Kanagawa 259-1193, Japan

⁷Department of Pathology, Tokai University School of Medicine, Isehara, Kanagawa 259-1193, Japan

⁸Department of Psychiatry, Nagoya University Graduate School of Medicine, Nagoya, Aichi 466-8550, Japan

⁹Medical Genomics Center, Nagoya University Hospital, Nagoya, Aichi 466-8550, Japan

¹⁰Tokyo Metropolitan Matsuzawa Hospital, Setagaya, Tokyo 156-0057, Japan

¹¹Tokyo Metropolitan Institute of Medical Science, Setagaya, Tokyo 156-8506, Japan

Correspondence to: Ryuta Mizutani

Department of Bioengineering, Tokai University

Hiratsuka, Kanagawa 259-1292, Japan

Phone: +81-463-63-4455

E-mail: mizutanilaboratory@gmail.com

Abstract

Human mentality develops with age and is altered in psychiatric disorders, though their underlying mechanism is unknown. In this study, we analyzed nanometer-scale three-dimensional structures of brain tissues of the anterior cingulate cortex from eight schizophrenia and eight control cases. The distribution profiles of neurite curvature of the control cases showed a trend depending on their age, resulting in an age-correlated decrease in the standard deviation of neurite curvature (Pearson's $r = -0.80$, $p = 0.018$). In contrast to the control cases, the schizophrenia cases deviate upward from this correlation, exhibiting a 60% higher neurite curvature compared with the controls ($p = 7.8 \times 10^{-4}$). The neurite curvature also showed a correlation with a hallucination score (Pearson's $r = 0.80$, $p = 1.8 \times 10^{-4}$), indicating that neurite structure is relevant to brain function. We suggest that neurite curvature plays a pivotal role in brain aging and can be used as a hallmark to exploit a novel treatment of schizophrenia. This nano-CT paper is the result of our decade-long analysis and is unprecedented in terms of number of cases.

Introduction

Human mentality changes with age and matures even through adulthood. This depends on a wide variety of factors, such as genetic background, education, and lifestyle (Richards & Hatch, 2011). These factors in life course should affect the brain, including brain areas that exert mental functions. The volumetric decrease of grey matter gradually progresses with age (Esiri, 2007; Blinkouskaya et al., 2021), indicating that some microscopic changes occur in human brain tissue. Since loss of cortical neurons is not predominant in normal aging (Terry et al., 1987; Pakkenberg & Gundersen, 1997; Uylings & de Brabander, 2002; Pannese, 2011; von Bartheld, 2018), the decrease in grey matter volume should be attributed to other factors, such as morphological alteration of neurons (Pannese, 2011; von Bartheld, 2018). Indeed, microscopic studies of human cortical neurons have revealed significant regression of dendritic arbors with age (de Brabander et al., 1998; Pannese, 2011; Sikora et al., 2021). However, age-related neuronal alteration and its relation to mental function are not fully understood.

Schizophrenia is a mental disorder showing psychiatric symptoms including hallucinations and social withdrawal. Since schizophrenia onset peaks at young adult ages (Ochoa et al., 2012; Musket et al., 2020), brain development and aging should be relevant to the etiology of schizophrenia. Macroscopic brain changes, such as ventricular dilation, have been repeatedly observed in schizophrenia (Wright et al., 2000; Shenton et al., 2001; Olabi et al., 2011; Tang et al., 2012; Haijma et al., 2013; Kaur et al., 2020). Although the macroscopic changes in the brain should originate from microscopic alterations in the brain tissue, the neuropathology of schizophrenia remains unclarified (Bogerts, 1993; Harrison, 1999; Iritani, 2013).

We recently reported nanometer-scale three-dimensional analyses of post-mortem brain tissues of schizophrenia and control cases (Mizutani et al., 2019; 2021). The results of the analysis indicated that neurite curvature differs between individuals and becomes extraordinary in schizophrenia. In this study, we further analyzed brain tissues of the Brodmann area 24 (BA24) of the anterior cingulate cortex of schizophrenia and control cases by using synchrotron radiation nanotomography (nano-CT). In conjunction with our previous results, the geometric analysis of the neuronal structures of eight schizophrenia and eight control cases revealed significant differences between the schizophrenia and control groups for a number of structural parameters. The neuronal structure was also examined by taking account of age and a hallucination score in order to reveal possible relations between the neuronal structure and clinical information.

Results

Three-dimensional visualization and structural analysis

A three-dimensional visualization of brain tissues of four schizophrenia (S5-S8) and four control cases (N5-N8; Supplementary Table S1) was performed by using synchrotron radiation nano-CT (Supplementary Table S2), as previously reported for four other schizophrenia (S1-S4) and four control cases (N1-N4; Supplementary Table S3; Mizutani et al., 2019). The obtained three-dimensional images of neurons were traced to build Cartesian coordinate models of neurons (Mizutani et al., 2013; Supplementary Figures S1, S2, and S3). Figure 1 shows a schematic representation of

the nano-CT analysis. The figure also shows a three-dimensional image of a neuron of the S8 case and its model built by tracing the image.

The obtained coordinate models are composed of approximately 140 mm of neurite traces in total (Supplementary Table S1). Their three-dimensional coordinates were used for calculating the geometric parameters of the neuronal network, such as curvature, which is the reciprocal of the curve radius. Statistics of the geometric parameters are summarized in Supplementary Tables S1, S3, and S4.

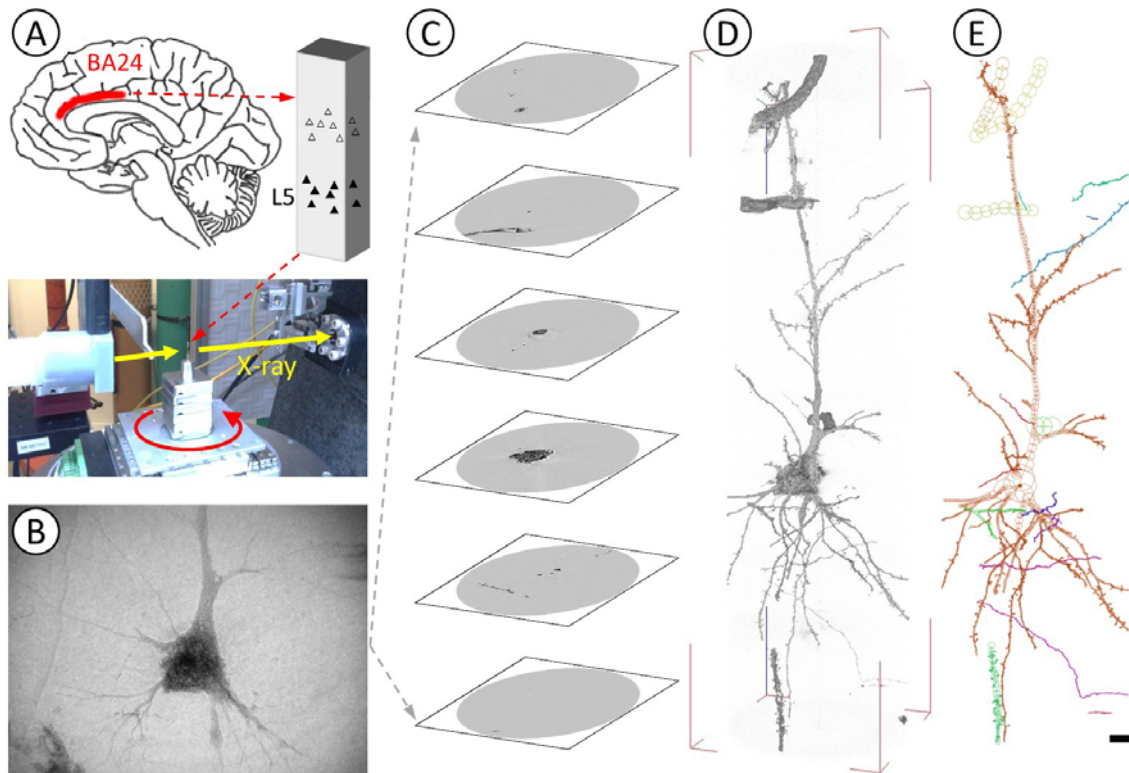


Figure 1. Nano-CT analysis of human brain neurons. **(A)** Brain tissues of Brodmann area 24 (BA24) of the anterior cingulate cortex were stained using the Golgi method and mounted on the sample stage of synchrotron radiation nano-CT. **(B)** A series of X-ray images of layer V neurons were taken while rotating the sample. This data collection process was repeated by shifting the sample along the sample rotation axis so as to cover the region of interest. **(C)** Tomographic slices were reconstructed from the image series and then stacked to obtain a three-dimensional image of the neuron. **(D)** Three-dimensional rendering of dataset S8A of the schizophrenia S8 case (Supplementary Table S4). Voxel values 60-800 were rendered with the scatter HQ algorithm of the VG Studio Max software (Volume Graphics, Germany). **(E)** The three-dimensional image was traced to build a Cartesian coordinate model by using the MCTrace software (Mizutani et al., 2013). Geometric parameters were calculated from the resultant three-dimensional coordinates. Structural constituents are color-coded. Nodes composing the model are depicted as circles. Scale bar: 10 μm .

Structure of control cases

The analysis of the obtained geometric parameters along with our previous results (Mizutani et al., 2019) indicated that the distribution of neurite curvatures of the control cases varies depending on their age. Figure 2A shows bee-swarm plots of the neurite curvature of the control cases. The plots illustrate that (1) the curvature maximum decreases as age increases and that (2) the curvature median increases as age increases. The decrease in the maximum curvature leads to an age-dependent decrease in the distribution span (Figure 2A), giving rise to a decrease in the standard deviation by age (Figure 2B). This age-dependent distribution resulted in a significant correlation between age and the standard deviation of neurite curvature (Figure 2B; Pearson's $r = -0.80$, $p = 0.018$). Since schizophrenia cases deviate upward from the correlation (Figure 2B), the age-related change in the control cases is opposite to the alteration in schizophrenia.

The bee-swarm plots of the neurite curvature of the control cases (Figure 2A) also illustrated that the distribution profiles of the control cases in the 40s exhibit vertically-symmetric spindle shapes, where the profiles of the older cases differ between individuals and hence are unique to each case. This suggests that the neurites of the control cases underwent structural changes during aging in different ways for each case.

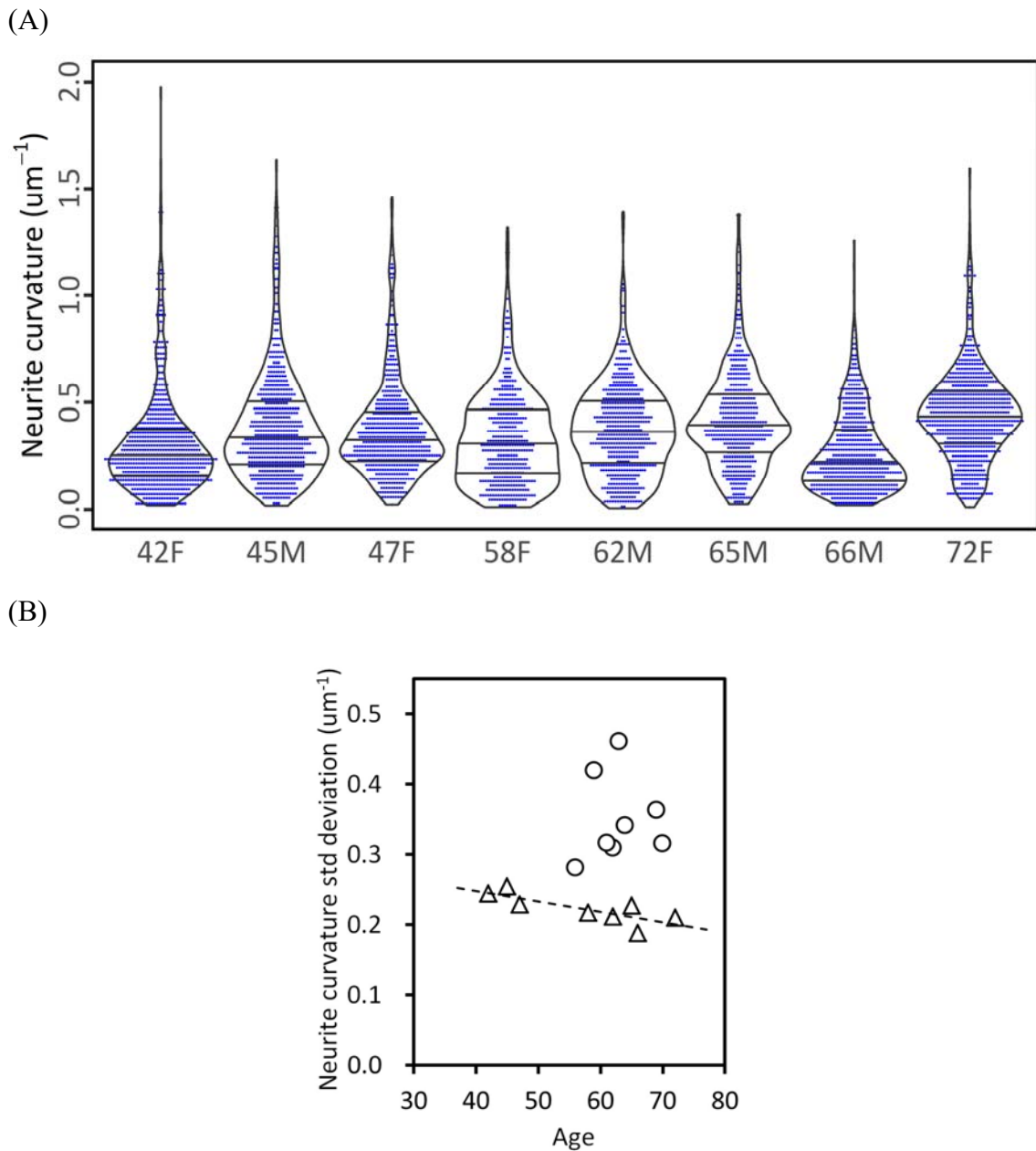


Figure 2. Relation between neurite curvature and age. **(A)** Bee-swarm and violin plots of neurite curvature of control cases. Each neurite is indicated with a blue dot. Cases are labeled with their age and sex. Quartiles are indicated with bars. Curvature maximum decreases with age, resulting in a decrease in the distribution span due to aging. This age-dependent decrease in the span leads to a correlation in panel B. **(B)** Scatter plot of standard deviation of neurite curvature versus age. Control cases are plotted with triangles and schizophrenia cases with circles. The dashed line indicates a linear regression (Pearson's $r = -0.80$, $p = 0.018$).

Structural differences between schizophrenia and control groups

The nano-CT analysis also revealed significant differences in the structural parameters between the schizophrenia and control groups. The neurite curvature of the schizophrenia group is significantly higher than that of the control group (Figure 3A; $p = 7.8 \times 10^{-4}$, Welch's t -test), resulting in a group mean ($0.58 \mu\text{m}^{-1}$) 60% higher than that of the controls ($0.36 \mu\text{m}^{-1}$). As observed in the age-dependence plot (Figure 2B), the standard deviation of neurite curvature is significantly higher in the schizophrenia cases compared with the controls ($p = 3.8 \times 10^{-4}$, Welch's t -test). The neurites of the schizophrenia cases are significantly thinner than those of the controls (Figure 3B; $p = 0.028$, Welch's t -test). The neurite thinning and curvature increase in schizophrenia cases coincides with our previous observation that neurite thickness inversely correlates with neurite curvature (Mizutani et al., 2019, 2021).

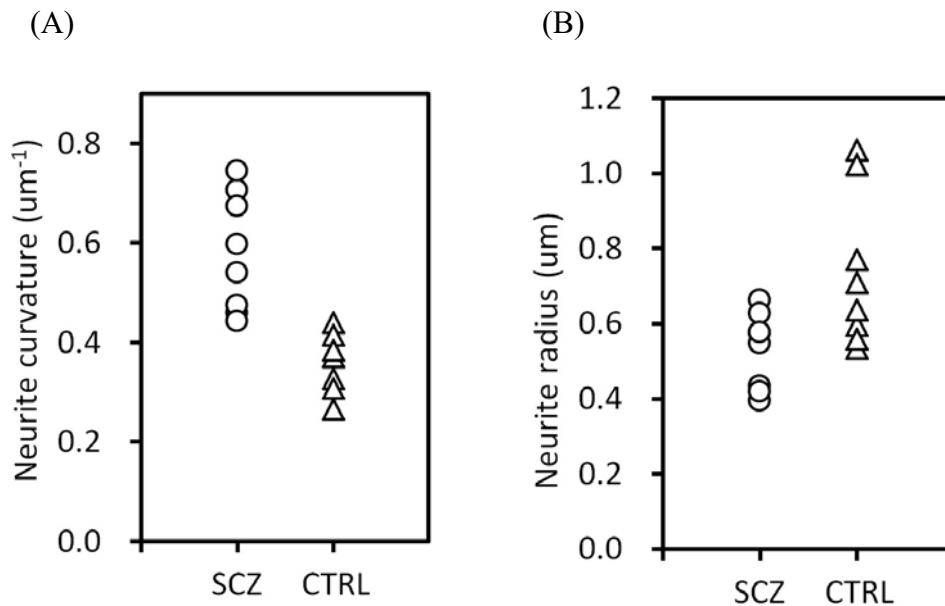


Figure 3. Differences in structural parameters between schizophrenia and control groups. (A) Neurite curvature ($p = 7.8 \times 10^{-4}$, Welch's t -test). (B) Neurite radius ($p = 0.028$, Welch's t -test).

These structural differences between the schizophrenia and control groups originated from differences in the distribution profiles of neurite curvature. Figure 4A shows the frequency distribution of the neurite curvatures of the schizophrenia cases. The plots exhibit long tails representing the tortuous and thin network of schizophrenia (Figure 4C). In contrast, the control cases showed almost no distribution beyond $0.8 \mu\text{m}^{-1}$ in neurite curvature (Figure 4B), representing a rather smooth and thick network (Figure 4D). The parameter differences between the schizophrenia and control groups (Figure 2 and 3) are due to these structural differences.

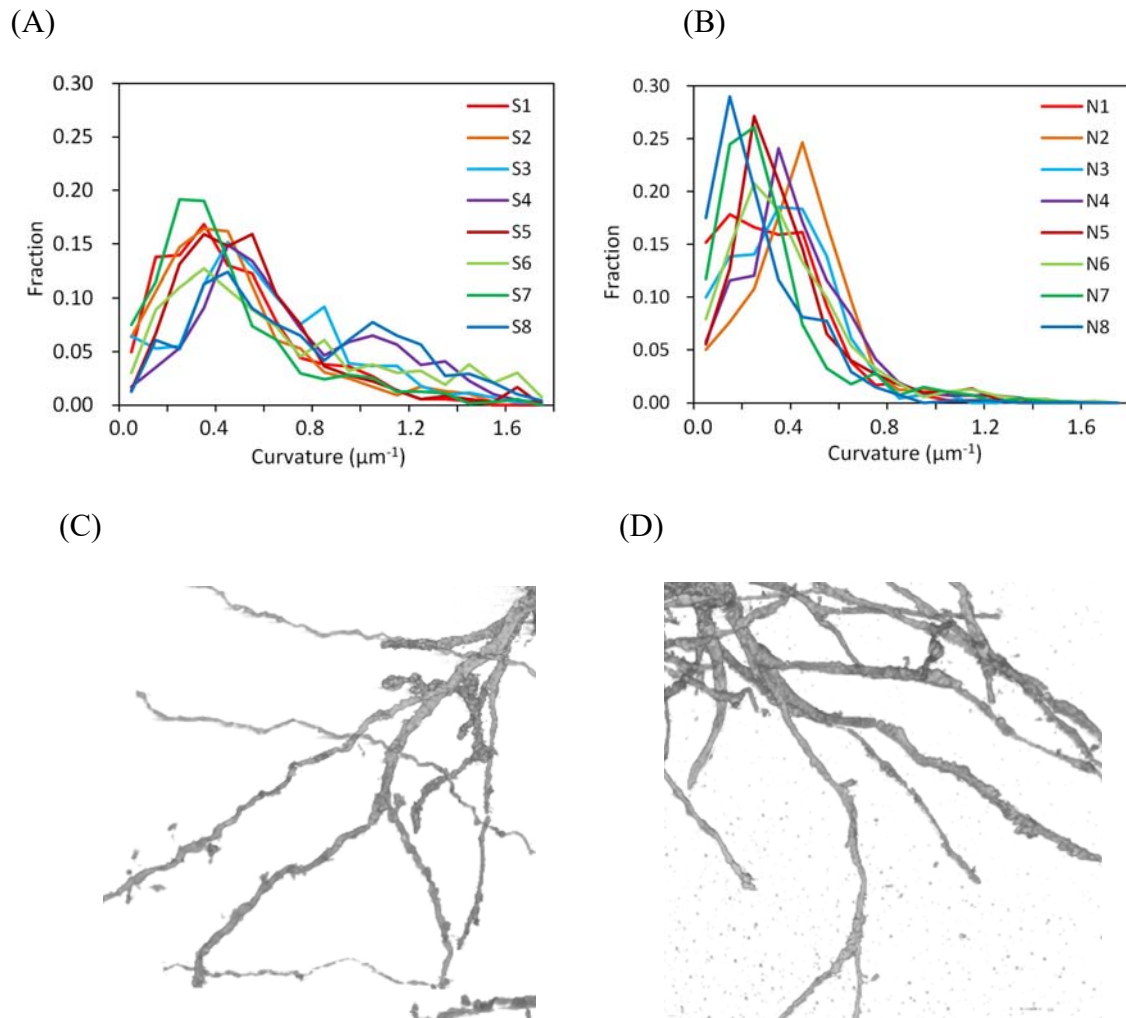


Figure 4. Differences in neurite structure between schizophrenia and control cases. **(A)** Frequency distribution of neurite curvatures of schizophrenia cases. Relative frequency in each $0.1 \mu\text{m}^{-1}$ bin of curvature is plotted. Cases are color-coded. The distribution shows a long tail for every schizophrenia case. **(B)** Frequency distribution of neurite curvature of control cases. The distribution beyond $0.8 \mu\text{m}^{-1}$ is negligible for every control case. **(C)** Three-dimensional rendering of neurites of the schizophrenia S8A structure. Voxel values 100-800 were rendered with the scatter HQ algorithm of VG Studio Max. Image width: $35 \mu\text{m}$. **(D)** Rendering of neurites of the control N5A structure at the same scale.

Neurite curvature correlates with hallucination score

Figure 5 shows a scatter plot of neurite curvature and auditory hallucination score. The plot indicated a significant correlation (Pearson's $r = 0.80$, $p = 1.8 \times 10^{-4}$), showing that the neuron structure correlates with the psychiatric symptom. We suggest that the hallucination severity can be estimated from a structural analysis of brain tissue by using this plot. No obvious correlation was found between the structural parameters and chlorpromazine equivalent dose (Supplementary Figure S4). This indicates that the structural changes observed in schizophrenia cases cannot be explained solely from the medication.

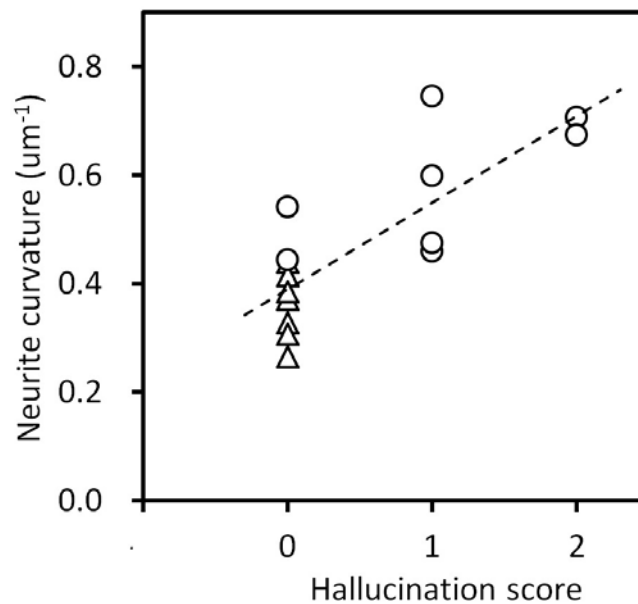


Figure 5. Scatter plot of neurite curvature and auditory hallucination score. Schizophrenia cases are plotted with circles and controls with triangles. The dashed line indicates a linear regression (Pearson's $r = 0.80$, $p = 1.8 \times 10^{-4}$).

Discussion

The standard deviation of the neurite curvature of the control cases showed a significant correlation with their age (Figure 2B). The distribution profiles of the neurite curvature suggested that the curvature distribution changed due to aging from vertically-symmetric profiles to case-specific profiles (Figure 2A). It has been discussed that the volumetric change in brain tissue due to aging (Esiri, 2007; Blinkouskaya et al., 2021) can be ascribed not only to loss of neurons (Terry et al., 1987; Pakkenberg & Gundersen, 1997; Uylings & de Brabander, 2002), but also to morphological changes in neurons (Pannese, 2011; von Bartheld, 2018). Since most of the electrophysiological properties of neurons, such as resting membrane potential and duration of action potential, remain the same during aging (Burke & Barnes, 2006), the morphological changes themselves should contribute to the aging of brain function. The age-structure correlation found in this study may be one of the factors affecting aging of the brain. The correlation between the psychiatric score and the structural parameter (Figure 5) suggests that the age-related structural change should have an effect on brain function.

The comparison of the schizophrenia and control groups revealed significant differences in structural parameters (Figure 3). A major difference was observed in the distribution profiles of neurite curvature (Figure 4), suggesting that neurons suffered structural changes from the disorder. The thickness of neurites also showed a significant difference between the schizophrenia and control groups, resulting in thinner neurites in schizophrenia (Figure 3B). According to cable theory (Hansson et al., 1994), neurite thinning should hinder the transmission of active potentials especially between distal neurons. A simulation study using an artificial neural network (Mizutani et al., 2022) indicated that a moderate suppression of distal connections improves network

performance, though excess suppression degrades network function. We suggest that the tortuous and thin neurites observed in the schizophrenia cases affected the performance of their cortical network of the anterior cingulate cortex that exerts emotional and cognitive functions (Botvinick et al., 1999; Bush et al., 2000).

Schizophrenia has historically been considered to be a progressive brain disorder according to Kraepelin's definition of *dementia praecox* at the end of 19th century (DeLisi, 2008). However, longitudinal studies of clinical outcomes and MRI brain volumes have indicated that schizophrenia cannot be considered to be solely a progressive disorder (Zipursky et al., 2013). In this study, we found that the age-related change in the control cases is opposite to the alteration in the schizophrenia cases, of which neurite curvature showed no obvious age dependence (Figure 2B). This indicates that the neuronal alteration in schizophrenia is different from that which occurs during normal aging. Indeed, the analysis of gene expression profiles showed that the expression trajectory during aging of schizophrenia cases is different from the age-related change of controls (Sabunciyan, 2019). Since cognitive functioning in schizophrenia does not appear to deteriorate over time (Reichenberg et al., 2010; Russell et al., 1997), we suggest that the idea of schizophrenia being a progressive disorder should be re-examined by taking account of recent findings.

The schizophrenia S8 case carrying a chromosome 22q11.2 deletion (Torii et al., 2020) showed the highest neurite curvature ($0.74 \mu\text{m}^{-1}$) among all the cases analyzed in this study (Supplementary Table S3). The second highest curvature ($0.71 \mu\text{m}^{-1}$) was observed in the S4 case carrying a *GLO1* mutation (Arai et al., 2010, 2014). These mutations should be one of the factors that altered the neuronal structures. The 22q11.2 deletion is relevant to neurological disorders such as epilepsy and movement disorders

and increases the risk of schizophrenia (Bayat & Bayat, 2022). Radiographic studies of the 22q11.2 deletion syndrome revealed brain malformations (Bohm et al., 2017), suggesting that this syndrome accompanies histological changes in brain tissue. The *GLO1* gene has also been identified as a susceptible locus relevant to schizophrenia (Arai et al., 2010; Yin et al., 2021). Genetic defects in *GLO1* increase the risk of carbonyl stress and showed a correlation with negative symptoms (Itokawa et al., 2014). Although genome-wide studies of psychiatric disorders identified a number of disorder-related genes (Horwitz et al., 2019), underlying mechanisms linking the mutations to the disorders have not been delineated. The two highest curvatures of the mutation cases of this study indicate that neuronal structure should be examined also for other mutations relevant to schizophrenia. We suggest that neuronal structural change plays a pivotal role in linking susceptible genes and disorder symptoms.

It has been reported that the anterior cingulate cortex shows a grey matter reduction in schizophrenia (Bouras et al., 2001; Fornito et al., 2009; Bersani et al., 2014) and is associated with auditory hallucinations in schizophrenia (Shergill et al., 2000; Rajj et al., 2009). Therefore, brain tissue alteration related to the auditory hallucination should reside in the anterior cingulate cortex of schizophrenia sufferers. In this study, the neurite curvature of this brain area showed a correlation with auditory hallucination score (Figure 5). This result suggests that the hallucination can be reduced by decreasing neurite curvature in the anterior cingulate cortex. Although a methodology to manipulate neuron structure of a specific brain area is currently unavailable, neurite curvature can be used as a hallmark with which to exploit antipsychotics or other interventions that can moderate hallucinations. Structural analysis of human brain neurons in other areas will further reveal the relation between the structure and function

of neuronal networks and hence will provide information beneficial to sufferers of psychiatric disorders.

There still remains a possibility that the structural changes to neurons observed in schizophrenia cases are caused by antipsychotics, though no obvious correlation was observed between structural parameters and antipsychotic dose (Supplementary Figure S4). Another limitation of this study is that the analyzed cases are small groups composed of Japanese sufferers. Further analysis of a larger cohort having other racial backgrounds should be conducted to generalize the findings of this study.

Subjects and Methods

Cerebral tissues

All post-mortem human cerebral tissues were collected with informed consent from the legal next of kin using protocols approved by the Clinical Study Reviewing Board of Tokai University School of Medicine (application no. 07R-018) and the Ethics Committee of Tokyo Metropolitan Institute of Medical Science (approval nos. 17-18 and 20-19). This study was conducted under the approval of the Ethics Committee for the Human Subject Study of Tokai University (approval nos. 11060, 11114, 12114, 13105, 14128, 15129, 16157, 18012, 19001, 20021, 20022, 21008, 21009, 22009, and 22010). The number of cases used for the analysis was determined from the available beamtime at synchrotron radiation facilities. Schizophrenia patients S1–S4 and controls N1–N4 are the same as in our previous study (Mizutani et al., 2019). Schizophrenia patients S5–S8 (Supplementary Table S1) were diagnosed according to the DSM-IV criteria by at least two experienced psychiatrists. The S8 case carried a chromosome 22q11.2 deletion (Torii et al., 2020). Auditory hallucination scores of the S1–S8 cases were estimated with the Present State Examination (PSE; Wing et al., 1974) without structural analysis information. Control patients N5–N8 (Supplementary Table S1) were hospitalized due to sudden death (N7) or non-psychiatric diseases (N5, N6, and N8) and were not psychiatrically evaluated. No records of schizophrenia were found for the control cases. Auditory hallucination scores of the control cases were estimated to be zero (Pomarol-Clotet et al., 2006).

Tissues of the anterior cingulate cortex (Brodmann area 24) were dissected from the left hemispheres of the autopsied brains of the schizophrenia and control cases. Histological

assessment of the cerebral tissues showed no hemorrhage, infarction, or neoplasm. The tissues were subjected to Golgi impregnation and embedded in epoxy resin using borosilicate glass capillaries, as reported previously (Mizutani et al., 2019).

Microtomography and nanotomography

The overall structure of the resin-embed samples was visualized with simple projection microtomography at the BL20XU beamline (Suzuki et al., 2004) of SPring-8. The data collection conditions are summarized in Supplementary Table S2. Absorption contrast images were acquired using CMOS imaging detectors (ORCA-Flash2.8 and ORCA-Flash4.0, Hamamatsu Photonics, Japan) as reported previously (Mizutani et al., 2019). Three-dimensional images of the tissue samples were reconstructed from the obtained x-ray images and used to locate layer V positions to find neurons. Examples of overall images of tissue samples are shown in Supplementary Figure S5.

Each neuron was then visualized with synchrotron radiation nanotomography (nano-CT) equipped with Fresnel zone plate optics (Takeuchi et al., 2002). The nano-CT experiments were conducted as reported previously (Mizutani et al., 2019, 2021) at the BL37XU (Suzuki et al., 2016) and the BL47XU (Takeuchi et al., 2009) beamlines of the SPring-8 synchrotron radiation facility, and at the 32-ID beamline (De Andrade et al., 2016, 2021) of the Advanced Photon Source (APS) of Argonne National Laboratory. The data collection conditions are summarized in Supplementary Table S2. Photon flux at the sample position was determined to be 1.4×10^{14} photons/mm²/s at BL37XU or 1.5×10^{14} photons/mm²/s at 32-ID by using Al₂O₃:C dosimeters (Nagase-Landauer, Japan). Spatial resolutions were estimated from the Fourier domain plot (Mizutani et al., 2016) or by using three-dimensional test patterns (Mizutani et al., 2008).

Structural analysis

Tomographic reconstruction of the obtained datasets were performed with the convolution-back-projection method using the RecView software (RRID: SCR_016531; Mizutani et al., 2010), as reported previously (Mizutani et al., 2019). The reconstruction calculation was conducted by RS. The resultant image datasets were provided to RM without case information in order to eliminate human biases in the structural analysis. RM built three-dimensional coordinate models of tissue structures by tracing the reconstructed images with the MCTrace software (RRID: SCR_016532; Mizutani et al., 2013). Coordinate files of the resultant structural models in Protein Data Bank format were locked down after the model building of each dataset was finished. Then, RM reported the number of neurite segments to RS only by stating that the number should be aggregated into each case. RS aggregated the numbers in order to find cases in which the analysis amounts were less than others. The aggregation

results were not returned to RM. Datasets to be further analyzed were chosen by RS according to the aggregation results and provided to RM without case information. These model-building and result aggregation processes were repeated for five batches. Since the first batch consisting of datasets S7A, S7B, S7C, N6F, N6G, N6H, N6I, N7E, N7F, N7G, and N7H was analyzed at the early stage of this study, their case information was disclosed to RM after the model building of the first batch was finished in order to examine the feasibility of the analysis process. The other four batches were continuously analyzed without case information. After the model building of the four batches was finished, all case information was disclosed to RM to assign datasets to each case.

Since eight dummy datasets unrelated to this study were included in order to shuffle datasets, those dummy sets were not used in the subsequent analysis. All other 54 datasets were subjected to geometric analysis. Structural parameters were calculated from three-dimensional Cartesian coordinates by using the MCTrace software, as reported previously (Mizutani et al., 2019). Statistics of the obtained structural parameters are summarized in Supplementary Tables S1, S3, and S4.

Code availability

RecView software (RRID: SCR_016531) and its source code used for the tomographic reconstruction are available from <https://mizutanilab.github.io> under the BSD 2-Clause License. The model building and geometric analysis were performed using the MCTrace software (RRID: SCR_016532) available from the same location under the BSD 2-Clause License.

Statistical tests

Statistical tests of the structural parameters were performed using the R software. Significance was defined as $p < 0.05$. Differences in structural parameters between groups were examined using Welch's *t*-test. Correlations between structural parameters and clinical information were examined by using linear regression analysis along with Pearson's correlation coefficient.

Acknowledgements

We are grateful to Prof. Motoki Osawa and Akio Tsuboi (Tokai University School of Medicine) for their generous support of this study. We also thank the Technical Service Coordination Office of Tokai University for assistance in preparing sample adapters for nanotomography. The analysis of human tissues was conducted under the approval of the Ethics Committee for the

Human Subject Study of Tokai University, the Clinical Study Reviewing Board of Tokai University School of Medicine, the Ethics Committee of Tokyo Metropolitan Institute of Medical Science, and the Institutional Biosafety Committee of Argonne National Laboratory. This research was supported by the Japan Agency for Medical Research and Development (JP21wm0425007 and JP21dk0307103 to NO, JP19km0405216 and JP22tm0424222 to IK, and JP22wm0425019 to Y Torii) and by the Japan Society for the Promotion of Science (20K20602 and 21H04815 to NO, and 21K07543 and 21H00194 to IK). The synchrotron radiation experiments at SPring-8 were performed with the approval of the Japan Synchrotron Radiation Research Institute (JASRI) (proposal nos. 2011A0034, 2014A1057, 2015A1160, 2019B1087, 2020A0614, 2020A1163, and 2021A1175). The synchrotron radiation experiment at the Advanced Photon Source of Argonne National Laboratory was performed under General User Proposal GUP-59766. This research used resources of the Advanced Photon Source, a U.S. Department of Energy (DOE) Office of Science User Facility operated for the DOE Office of Science by Argonne National Laboratory under Contract No. DE-AC02-06CH11357.

Author Contributions

RM designed the study. RM, RS, ST, CI, NN, Y Torii, IK, SI, NO, KO, MI, and MA prepared the samples. CI, NN, Y Torii, IK, SI, NO, KO, and MI examined the clinical information. RM, RS, MU, AT, KU, Y Terada, YS, VDA, and FDC performed the synchrotron radiation experiments. RM, RS, and YY analyzed the data. RM wrote the manuscript and prepared the figures. All authors reviewed the manuscript.

Conflict of interest

MI and MA declare a conflict of interest, being authors of several patents regarding therapeutic use of pyridoxamine for schizophrenia. All other authors declare no conflict of interest.

References

1. M. Richards, S. L Hatch, A life course approach to the development of mental skills. *J. Gerontol. B Psychol. Sci. Soc. Sci.* **66** (suppl. 1), i26–35 (2011).
2. M. M. Esiri, Ageing and the brain. *J. Pathol.* **211**, 181–187 (2007).
3. Y. Blinkouskaya, A. Caçoilo, T. Gollamudi, S. Jalalian, J. Weickenmeier, Brain aging mechanisms with mechanical manifestations. *Mech. Ageing Dev.* **200**, 111575 (2021).
4. R. D. Terry, R. DeTeresa, L. A. Hansen, Neocortical cell counts in normal human adult aging. *Ann. Neurol.* **21**, 530–539 (1987).
5. B. Pakkenberg, H. J. Gundersen, Neocortical neuron number in humans: effect of sex and age. *J. Comp. Neurol.* **384**, 312–320 (1997).

6. H. B. M. Uylings, J. M. de Brabander, Neuronal changes in normal human aging and Alzheimer's disease. *Brain Cogn.* **49**, 268–276 (2002).
7. E. Pannese, Morphological changes in nerve cells during normal aging. *Brain Struct. Funct.* **216**, 85–89 (2011).
8. C. S. von Bartheld, Myths and truths about the cellular composition of the human brain: a review of influential concepts. *J. Chem. Neuroanat.* **93**, 2–15 (2018).
9. J. M. de Brabander, R. J. Kramers, H. B. Uylings, Layer-specific dendritic regression of pyramidal cells with ageing in the human prefrontal cortex. *Eur. J. Neurosci.* **10**, 1261–1269 (1998).
10. E. Sikora, A. Bielak-Zmijewska, M. Dudkowska, A. Krzystyniak, G. Mosieniak, M. Wesierska, J. Wlodarczyk, Cellular senescence in brain aging. *Front. Aging Neurosci.* **13**, 646924 (2021).
11. Susana Ochoa, Judith Usall, Jesús Cobo, Xavier Labad, Jayashri Kulkarni, Gender differences in schizophrenia and first-episode psychosis: A comprehensive literature review. *Schizophr. Res. Treatment* **2012**, 916198 (2012).
12. C. W. Musket, S. S. Kuo, P. E. Rupert, L. Almasy, R. C. Gur, K. Prasad, J. Wood, D. R. Roalf, R. E. Gur, V. L. Nimgaonkar, M. F. Pogue-Geile, Why does age of onset predict clinical severity in schizophrenia? A multiplex extended pedigree study. *Am. J. Med. Genet. B Neuropsychiatr. Genet.* **183**, 403–411 (2020).
13. I. C. Wright, S. Rabe-Hesketh, P. W. Woodruff, A. S. David, R. M. Murray, E. T. Bullmore, Meta-analysis of regional brain volumes in schizophrenia. *Am. J. Psychiatry* **157**, 16–25 (2000).
14. M. E. Shenton, C. C. Dickey, M. Frumin, R. W. McCarley, A review of MRI findings in schizophrenia. *Schizophr. Res.* **49**, 1–52 (2001).
15. B. Olabi, I. Ellison-Wright, A. M. McIntosh, S. J. Wood, E. Bullmore, S. M. Lawrie, Are there progressive brain changes in schizophrenia? A meta-analysis of structural magnetic resonance imaging studies. *Biol. Psychiatry* **70**, 88–96 (2011).
16. J. Tang, Y. Liao, B. Zhou, C. Tan, W. Liu, D. Wang, T. Liu, W. Hao, L. Tan, X. Chen, Decrease in temporal gyrus gray matter volume in first-episode, early onset schizophrenia: an MRI study. *PLoS One* **7**, e40247 (2012).
17. S. V. Haijma, N. van Haren, W. Cahn, P. C. M. P. Koolschijn, H. E. H. Pol, R. S. Kahn, Brain volumes in schizophrenia: a meta-analysis in over 18,000 subjects. *Schizophr. Bull.* **39**, 1129–1138 (2013).
18. A. Kaur, D. M. Basavanagowda, B. Rathod, N. Mishra, S. Fuad, S. Nosher, Z. A. Alrashid, D. Mohan, S. E. Heindl, Structural and functional alterations of the temporal lobe in schizophrenia: A literature review. *Cureus* **12**, e11177 (2020).

19. B. Bogerts, Recent advances in the neuropathology of schizophrenia. *Schizophr. Bull.* **19**, 431–445 (1993).
20. P.J. Harrison, The neuropathology of schizophrenia: A critical review of the data and their interpretation. *Brain* **122**, 593–624 (1999).
21. S. Iritani, What happens in the brain of schizophrenia patients? : an investigation from the viewpoint of neuropathology. *Nagoya J. Med. Sci.* **75**, 11–28 (2013).
22. R. Mizutani, R. Saiga, A. Takeuchi, K. Uesugi, Y. Terada, Y. Suzuki, V. De Andrade, F. De Carlo, S. Takekoshi, C. Inomoto, N. Nakamura, I. Kushima, S. Iritani, N. Ozaki, S. Ide, K. Ikeda, K. Oshima, M. Itokawa, M. Arai, Three-dimensional alteration of neurites in schizophrenia. *Transl. Psychiatry* **9**, 85 (2019).
23. R. Mizutani, R. Saiga, Y. Yamamoto, M. Uesugi, A. Takeuchi, K. Uesugi, Y. Terada, Y. Suzuki, V. De Andrade, F. De Carlo, S. Takekoshi, C. Inomoto, N. Nakamura, Y. Torii, I. Kushima, S. Iritani, N. Ozaki, K. Oshima, M. Itokawa. M. Arai, Structural diverseness of neurons between brain areas and between cases. *Transl. Psychiatry* **11**, 49 (2021).
24. R. Mizutani, R. Saiga, A. Takeuchi, K. Uesugi, Y. Suzuki, Three-dimensional network of *Drosophila* brain hemisphere. *J. Struct. Biol.* **184**, 271–279 (2013).
25. S. Burke, C. Barnes, Neural plasticity in the ageing brain. *Nat. Rev. Neurosci.* **7**, 30–40 (2006).
26. B. S. Hansson, E. Hallberg, C. Löfstedt, R. A. Steinbrecht, Correlation between dendrite diameter and action potential amplitude in sex pheromone specific receptor neurons in male *Ostrinia nubilalis* (Lepidoptera: Pyralidae). *Tissue Cell* **26**, 503–512 (1994).
27. R. Mizutani, S. Noguchi, R. Saiga, Y. Yamashita, M. Miyashita, M. Arai, M. Itokawa, Schizophrenia-mimicking layers outperform conventional neural network layers. *Front. Neurobot.* **16**, 851471 (2022).
28. M. Botvinick, L. E. Nystrom, K. Fissell, C. S. Carter, J. D. Cohen, Conflict monitoring versus selection-for-action in anterior cingulate cortex. *Nature* **402**, 179–181 (1999).
29. G. Bush, P. Luu, M. I. Posner. Cognitive and emotional influences in anterior cingulate cortex. *Trends Cogn. Sci.* **4**, 215–222 (2000).
30. L. E. DeLisi, The concept of progressive brain change in schizophrenia: implications for understanding schizophrenia. *Schizophr. Bull.* **34**, 312–321 (2008).
31. R. B Zipursky, T. J. Reilly, R. M. Murray, The myth of schizophrenia as a progressive brain disease. *Schizophr. Bull.* **39**, 1363–1372 (2013).
32. S. Sabunciyani, Gene expression profiles associated with brain aging are altered in schizophrenia. *Sci. Rep.* **9**, 5896 (2019).
33. A. Reichenberg, A. Caspi, H. Harrington, R. Houts, R. S. E. Keefe, R. M. Murray, R. Poulton, T. E Moffitt, Static and dynamic cognitive deficits in childhood preceding adult

- schizophrenia: a 30-year study. *Am. J. Psychiatry* **167**, 160–169 (2010).
34. A. J. Russell, J. C. Munro, P. B. Jones, D. R. Hemsley, R. M. Murray, Schizophrenia and the myth of intellectual decline. *Am. J. Psychiatry* **154**, 635–639 (1997).
 35. Y. Torii, S. Iritani, T. Marui, H. Sekiguchi, C. Habuchi, H. Fujishiro, I. Kushima, K. Oshima, K. Niizato, S. Hayashida, K. Masaki, J. Kira, M. Yoshida, N. Ozaki, Morphological alteration of myelin-oligodendrocytes in a schizophrenic patient with 22q11.2 deletion syndrome: An autopsy study. *Schizophr. Res.* **223**, 353–355 (2020).
 36. M. Arai, H. Yuzawa, I. Nohara, T. Ohnishi, N. Obata, Y. Iwayama, S. Haga, T. Toyota, H. Ujike, M. Arai, T. Ichikawa, A. Nishida, Y. Tanaka, A. Furukawa, Y. Aikawa, O. Kuroda, K. Niizato, R. Izawa, K. Nakamura, N. Mori, D. Matsuzawa, K. Hashimoto, M. Iyo, I. Sora, M. Matsushita, Y. Okazaki, T. Yoshikawa, T. Miyata, M. Itokawa, Enhanced carbonyl stress in a subpopulation of schizophrenia. *Arch. Gen. Psychiatry* **67**, 589–597 (2010).
 37. M. Arai, A. Kobori, M. Miyashita, K. Toriumi, Y. Horiuchi, S. Hatakeyama, M. Itokawa, Pentosidine accumulation in the pathophysiology of schizophrenia: overview of schizophrenia with carbonyl stress. *IMARS Highlights* **9**, 9–16 (2014).
 38. M. Bayat, A. Bayat. Neurological manifestation of 22q11.2 deletion syndrome. *Neurol. Sci.* **43**, 1695–1700 (2022).
 39. L. A. Bohm, T. C. Zhou, T. J. Mingo, S. L. Dugan, R. J. Patterson, J. D. Sidman, B. B. Roby, Neuroradiographic findings in 22q11.2 deletion syndrome. *Am. J. Med. Genet. A* **173**, 2158–2165 (2017).
 40. J. Yin, G. Ma, S. Luo, X. Luo, B. He, C. Liang, X. Zuo, X. Xu, Q. Chen, S. Xiong, Z. Tan, J. Fu, D. Lv, Z. Dai, X. Wen, D. Zhu, X. Ye, Z. Lin, J. Lin, Y. Li, W. Chen, Z. Luo, K. Li, Y. Wang, Glyoxalase 1 confers susceptibility to schizophrenia: From genetic variants to phenotypes of neural function. *Front. Mol. Neurosci.* **14**, 739526 (2021).
 41. M. Itokawa, M. Miyashita, M. Arai, T. Miyata, Carbonyl stress in schizophrenia. *Biochem. Soc. Trans.* **42**, 468–472 (2014).
 42. T. Horwitz, K. Lam, Y. Chen, Y. Xia, C. Liu, A decade in psychiatric GWAS research. *Mol. Psychiatry* **24**, 378–389 (2019).
 43. C. Bouras, E. Kövari, P. R. Hof, B. M. Riederer, P. Giannakopoulos, Anterior cingulate cortex pathology in schizophrenia and bipolar disorder. *Acta Neuropathol.* **102**, 373–379 (2001).
 44. A. Fornito, M. Yücel, B. Dean, S. J. Wood, C. Pantelis, Anatomical abnormalities of the anterior cingulate cortex in schizophrenia: bridging the gap between neuroimaging and neuropathology. *Schizophr. Bull.* **35**, 973–993 (2009).
 45. F. S. Bersani, A. Minichino, M. Fojanesi, M. Gallo, G. Maglio, G. Valeriani, M. Biondi, P. B. Fitzgerald, Cingulate cortex in schizophrenia: its relation with negative symptoms and

- psychotic onset. A review study. *Eur. Rev. Med. Pharmacol. Sci.* **18**, 3354–3367 (2014).
46. S. S. Shergill, M. J. Brammer, S. C. Williams, R. M. Murray, P. K. McGuire, Mapping auditory hallucinations in schizophrenia using functional magnetic resonance imaging. *Arch. Gen. Psychiatry* **57**, 1033–1038 (2000).
 47. T. T. Rajj, M. Valkonen-Korhonen, M. Holi, S. Therman, J. Lehtonen, R. Hari, Reality of auditory verbal hallucinations. *Brain* **132**, 2994–3001 (2009).
 48. J. K. Wing, J. E. Cooper, N. Sartorius, *The Measurement and Classification of Psychiatric Symptoms* (Cambridge University Press, Cambridge, 1974).
 49. E. Pomarol-Clotet, G. D. Honey, G. K. Murray, P. R. Corlett, A. R. Absalom, M. Lee, P. J. McKenna, E. T. Bullmore, P. C. Fletcher, Psychological effects of ketamine in healthy volunteers. Phenomenological study. *Br. J. Psychiatry* **189**, 173–179 (2006).
 50. Y. Suzuki, K. Uesugi, N. Takimoto, T. Fukui, K. Aoyama, A. Takeuchi, H. Takano, N. Yagi, T. Mochizuki, S. Goto, K. Takeshita, S. Takahashi, H. Ohashi, Y. Furukawa, T. Ohata, T. Matsushita, Y. Ishizawa, H. Yamazaki, M. Yabashi, T. Tanaka, H. Kitamura, T. Ishikawa, Construction and commissioning of a 248 m-long beamline with X-ray undulator light source. *AIP Conference Proceedings* **705**, 344–347 (2004).
 51. A. Takeuchi, K. Uesugi, H. Takano, Y. Suzuki, Submicrometer-resolution three-dimensional imaging with hard x-ray imaging microtomography. *Rev. Sci. Instrum.* **73**, 4246–4249 (2002).
 52. Y. Suzuki, A. Takeuchi, Y. Terada, K. Uesugi, R. Mizutani, Recent progress of hard x-ray imaging microscopy and microtomography at BL37XU of SPring-8. *AIP Conference Proceedings* **1696**, 020013 (2016).
 53. A. Takeuchi, K. Uesugi, Y. Suzuki, Zernike phase-contrast x-ray microscope with pseudo-Kohler illumination generated by sectorized (polygon) condenser plate. *J. Phys. Conf. Ser.* **186**, 012020 (2009).
 54. V. De Andrade, A. Deriy, M. J. Wojcik, D. Gürsoy, D. Shu, K. Fezzaa, F. De Carlo, Nanoscale 3D imaging at the Advanced Photon Source. *SPIE Newsroom* 10.1117/2.1201604.006461 (2016).
 55. V. De Andrade, V. Nikitin, M. Wojcik, A. Deriy, S. Bean, D. Shu, T. Mooney, K. Peterson, P. Kc, K. Li, S. Ali, K. Fezzaa, D. Gürsoy, Fast X-ray nanotomography with sub-10 nm resolution as a powerful imaging tool for nanotechnology and energy storage applications. *Adv. Mater.* **33**, e2008653 (2021).
 56. R. Mizutani, R. Saiga, S. Takekoshi, C. Inomoto, N. Nakamura, M. Itokawa, M. Arai, K. Oshima, A. Takeuchi, K. Uesugi, Y. Terada, Y. Suzuki, A method for estimating spatial resolution of real image in the Fourier domain. *J. Microsc.* **261**, 57–66 (2016).
 57. R. Mizutani, A. Takeuchi, K. Uesugi, Y. Suzuki, Evaluation of the improved

three-dimensional resolution of a synchrotron radiation computed tomograph using a micro-fabricated test pattern. *J. Synchrotron Radiat.* **15**, 648–654 (2008).

58. R. Mizutani, A. Takeuchi, K. Uesugi, S. Takekoshi, R. Y. Osamura, Y. Suzuki, Microtomographic analysis of neuronal circuits of human brain. *Cereb. Cortex* **20**, 1739–1748 (2010).

This is a preprint version submitted to the arXiv repository. Supplementary Materials will be provided separately, probably from some journal site.